RSC Advances

ROYAL SOCIETY OF CHEMISTRY

www.rsc.org/advances

Cite this: DOI: 10.1039/c0xx00000x

www.rsc.org/xxxxxx

ARTICLE TYPE

Highly Efficient and Selective Degradation of Methylene Blue from Mixed Aqueous Solution by Using Monodisperse $CuFe_2O_4$ Nanoparticles

Lingyun Wang,[a,b] Guowen Hu,[b] Zhiyi Wang,[a] Baodui Wang,[b,*] Yumin Song,[a,*] and Huiang Tang,[c*]

Received (in XXX, XXX) Xth XXXXXXXXX 20XX, Accepted Xth XXXXXXXXX 20XX DOI: 10.1039/b000000x

It is still difficult to selectively remove the harmful pollutants from complicated wastewaters in the presence of other less-harmful pollutants. Methylene blue (MB) is a worldwide water contaminant that is currently without effective and selective agent to detect and degrade it. We present herein the design and synthesis of a monodisperse $CuFe_2O_4$ nanocatalyst for selective and rapid degradation of methylene blue (MB). In the presence of other pollutants such as methylene orange (MO), rhodamine B (RB) and rhodamine 6G (R6G), MB was still rapidly degraded. The catalyst could be easily separated and recycled without significant loss of catalytic activity after being used 10 times. The $CuFe_2O_4$ nanoparticles (NPs) could be a promising catalyst for selective degradation of synthetic dyes from their mixture.

1. Introduction

The design and synthesis of nanocatalysts for highly efficient and selective degradation the harmful pollutants from complicated waste water are extremely desirable for human health and environmental protection today. Methylene blue (MB) is one of the most commonly used dyes in various industries such as textiles, printing, rubber, etc.[1] The effluents from these industries are a major source of environmental pollution. Not only do water bodies become colored, but also environmental damage occurs to living organisms by decreasing the dissolved oxygen capacity of water and by blocking sunlight, thereby disturbing the natural growth activity of aquatic life. Nowadays, common effluent treatment methods including adsorption, photocatalytic degradation, chemical oxidation, membrane filtration, flocculation, and electro oxidation are difficult to remove the specific dye.[2,3] Thus it is necessary to find a desirable nanocatalyst which not only is able to degrade the pollutant organic dyes with high efficiency and low lost, but also realizes selective degradation, separation and recovery of raw material.

It is well-established that various nanocatalysts including metal oxides are widely used for the remediation of effluents in the dye industry.[4] Among those, some spinel-type transition-metal oxides have attracted much fundamental and applied research attention from the past decade due to their excellent catalytic properties, a simple yet efficient recovery protocol, and low cost.[5] Current environmental catalysis research has shown that the spinel-type transition-metal oxide catalysts are effective for nitrogen oxide (NOx) decomposition/reduction reaction,[6] and some may have excellent catalytic activity for simultaneous catalytic removal of NOx and diesel soot particulates.[6e,7c] Spinel-type $CuFe_2O_4$ and $CoFe_2O_4$ nanoparticles (NPs) are two most excellent spinel-type oxides for simultaneous catalytic removal of nitrogen oxides and diesel particulates.[7,8] However, $CuFe_2O_4$ NPs) as catalysts still have not been explored to selectively degrade the MB of waste water up to now, although they have exhibit great potential applications in various fields. With this in mind, we intend to design and synthesize monodispersed $CuFe_2O_4$ NPs, then further investigate their degradation behavior of MB from wastewater. We demonstrate that this catalyst showed high activity and selectivity toward MB in the presence of other pollutants such as methylene orange (MO), rhodamine B (RB) and rhodamine 6G (R6G) and could be easily separated from the reaction solution by an external magnetic field and reused 10 times without significant loss of catalytic activity. To the best of our knowledge, this is the first report that $CuFe_2O_4$ NPs was used in selective degradation of MB in the presence of other dyes.

2. Experimental section

2.1 Experimental Chemicals

Benzyl ether (15 mL), oleylamine (10 mL), Iron (III) acetylacetonate (1 mmol, 0.3531 g), Copper (II) acetylacetonate (1 mmol, 0.2618 g) were purchased from Sigma Aldrich. MB, MO, R6G and RB were obtained from Beijing Chemicals Inc (Beijing, China). All chemicals were used without further purification, except $CHCl_3$ and triethylamine were used anhydrously. Aqueous solutions were prepared with double-distilled water (ddH_2O) from a Millipore system (> 18 MΩ.cm). The 1, ω-Diaminopolyoxyethylene (MW = 4000) and DIB-PEG-NH_2 were synthesized according to the published method.[9] All the dialysis bags (MWCO 8000-14000) were obtained from Shanghai Med.

2.2 Instrumentation

TEM measurements were conducted with Philips EM 420 (120 kV) under ambient conditions with the deposition of the hexane or H_2O dispersions of the particles on amorphous carbon-coated copper grids. The hysteresis loop was obtained at 300K with a LakeShore 7400 VSM system. The UV-Vis absorbance measurement experiments were carried out on a UV-1750 spectrophotometer (Shimadzu, Japan). The Fourier Transform Infrared (FT-IR) spectra were recorded on a Therom Mattson FT-IR spectrometer using the KBr pellet technique. Powder X-ray Diffraction (XRD) analyses were performed on a Bruker AXS D8-Advanced diffractometer with Cu Ka radiation (λ = 1.5418 Å) and the scanning angle ranged from 10 to 110 of 2θ. Inductively Coupled Plasma-

Atomic Emission Spectrometry (ICP-AES) was executed with a FWS-1000.

2.3 Synthesis of $CuFe_2O_4$ nanoparticles.

A 100 mL four-necked round-bottomed flask was used in which Iron (III) acetylacetonate (1 mmol, 0.3531 g) and Copper (II) acetylacetonate (1 mmol, 0.2618 g) were dissolved in Benzyl ether (15 mL) and oleylamine (10 mL). The mixture was stirred under a gentle flow of nitrogen at 110 ^oC for 1.5 h. Then under a blanket of nitrogen, the solution was heated to reflux (300 ^oC) and kept at that temperature for 1 h. After it cooled down to room temperature, the particles were separated by adding 40 mL ethanol and centrifuging. The final products were washed by repeated actions of redispersion and subsequent precipitation with hexane/ethanol (V : V = 1 : 6) three times, and finally redispersed into hexane for storage.

2.4 Synthesis of $CuFe_2O_4$- DIB-PEG-NH_2 (1a) NPs.

In a 50 mL round-bottomed flask, DIB-PEG-NH_2 (0.025 mmol, 0.1 g) was dissolved in $CHCl_3$ (15-20 mL) at room temperature with continuous stirring. After a few minutes, the solution of $CuFe_2O_4$ NPs (0.001226 mmol, 2 mL) was dropwised into above solution and stirred 24 h at room temperature. The products were washed by petroleum ether and C_2H_5OH three times. The product was put into dialysis bags which were suspended in water for seven days. After that, the products were dissolved in ddH_2O.

2.5 Catalytic Activity Measurement.

The catalytic activity of the samples was determined by the degradation of MB, MO, R6G and RB with the help of $NaBH_4$. Experiments were conducted at ambient temperature as follows, unless otherwise stated: **1a** (Cu^{2+} 0.00805 mol/L) was added into ddH_2O (2 mL) containing the MB (1×10^{-5} mol, 20 μL) aqueous solution or equal-molar MO, R6G and RB aqueous solution. Then $NaBH_4$ (1×10^{-3} mol, 20 μL) was added to the above reaction mixture. At a given time interval (30 seconds), the concentrations of the remnant dye were recorded by measuring the absorbance of solution at 664 nm, 464 nm, 526 nm, and 552 nm during the degradation process on a UV-1750 spectrophotometer.

3. Results and discussion

3.1 Synthesis and Characteristics of $CuFe_2O_4$ NPs and $CuFe_2O_4$- DIB-PEG-NH_2 (1a)

$CuFe_2O_4$ NPs were synthesized *via* a facile thermal decomposition of $Fe(acac)_3$ and $Cu(acac)_2$ in a benzyl ether and oleylamine system. As can be seen from the TEM images (Fig. 1A), $CuFe_2O_4$ NPs coated with oleylamine exhibit nearly spherical morphology, a low degree of agglomeration and a narrow particle size distribution with an average size of 5.6 nm (inset in Fig. 1A). The high-resolution TEM (HRTEM) imaging (Fig. 1C) revealed that $CuFe_2O_4$ NPs had a relatively good crystal. The resolved lattice fringes of 0.327 nm agreed with the (311) facet of $CuFe_2O_4$ NPs.[10] The selected area electron diffraction (SAED) pattern (Fig. 1D) also confirmed the presence of $CuFe_2O_4$ NPs.[11] The energy-dispersive X-ray spectrum (EDX) analysis results show primarily O, Fe and Cu signals (Fig. 1F), suggesting that the $CuFe_2O_4$ NPs are formed. To further understand the crystal structures of $CuFe_2O_4$ NPs, an X-ray diffraction (XRD) analysis was conducted at the 2θ mode (Fig. 1G), which showed that the diffraction peaks at 30.2, 35.5, 43.3, 57.1 and 62.7° ascribed to (220), (311), (400), (511), and (440). The positions and relative intensities of all diffraction peaks matched well with the data of standard $CuFe_2O_4$ NPs (JCPDS Cards:77-10).[10a,11] To render these nanocrystal hydrophilic, the PEG-3,4-dihydroxy benzyl amine (DIB-PEG-NH_2) is grafted onto the as-prepared $CuFe_2O_4$ NPs via ligand exchange. No obvious change in the morphology of DIB-PEG-NH_2-grafted $CuFe_2O_4$ NPs (**1a**) is observed (Fig. 1B). The obtained **1a** was further confirmed by FT-IR spectra. In Fig. S1C, the absorption peaks at 1108 cm^{-1} was assigned to phenolic hydroxyl group of DIB-PEG-NH_2. After DIB-PEG-NH_2 was modified on $CuFe_2O_4$ NPs (Fig. S1A), the peak of the phenolic υ(C–O) at 1108 cm^{-1} is not observed. However, a new absorption peak of C–O–Cu and C–O–Fe vibration at 1048 cm^{-1} appears, indicating that the phenolic hydroxyl group of DIB-PEG-NH_2 are bound to the surface of $CuFe_2O_4$ NPs.[12,13] Also, the peak of υ(N-H) was shift from 1345 to 1340 cm^{-1} after forming **1a**. In addition, the absorption peak at 596 cm^{-1} could be assigned to the Fe-O and Cu-O bonds.[14-16] The compared photograph between before- and after-modification directly shows that hydrophobic $CuFe_2O_4$ NPs was well changed into hydrophilic **1a** by ligand-exchange chemistry (Fig. 1E). The good hydrophilic ability ensured the potential catalytic application in aqueous system. The magnetization curves in Fig. 2 showed that both $CuFe_2O_4$ NPs and **1a** were super-paramagnetic at room temperature, and **1a** in aqueous solution can be harvested and separated by a NdFeB magnet (inset in Fig. 2), which was extremely important for the magnetic separation and reusability of **1a** from the reaction mixture.

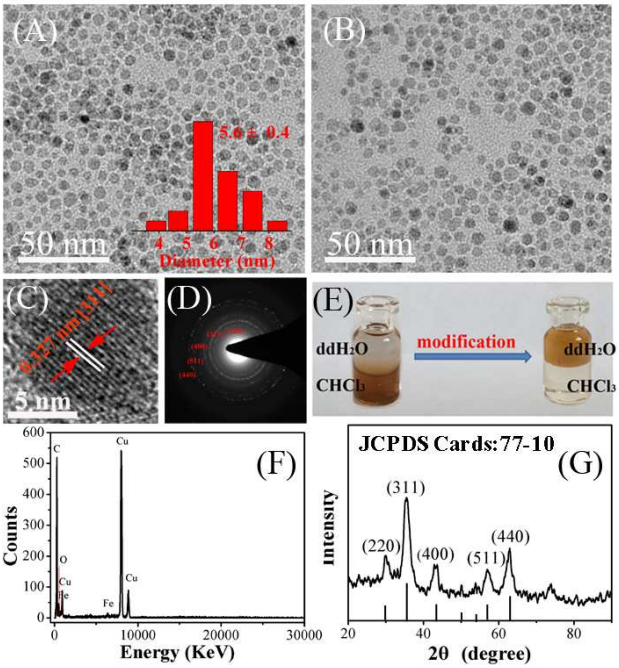

Fig. 1. (A) TEM image of $CuFe_2O_4$ NPs. The inset shows the size distribution histograms of $CuFe_2O_4$ NPs. (B) TEM image of **1a.** (C) HRTEM pattern of $CuFe_2O_4$ NPs. (D) SAED pattern of $CuFe_2O_4$ NPs. (E) The photograph of $CuFe_2O_4$ NPs between before- and after- modification. (F) EDX pattern of $CuFe_2O_4$ NPs indicating the presence of Cu, Fe, O. (G) The XRD spectra of $CuFe_2O_4$ NPs.

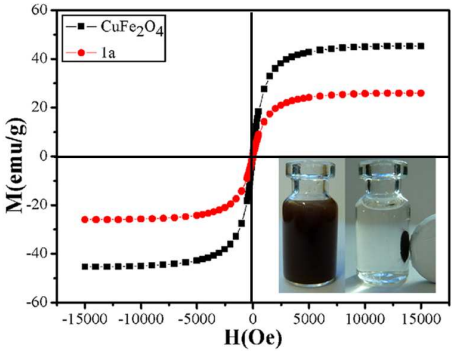

Fig. 2. Magnetic behavior of $CuFe_2O_4$ NPs and **1a** at 300 K. The photograph demonstrates that **1a** in aqueous solution can be attracted and arranged vertically by a NdFeB magnet.

3.2 Catalytic properties of the 1a catalyst

To evaluate the catalytic performance of **1a** for the degradation of dyes from contaminated water, MB, MO, R6G and RhB as the typical organic pollutant targets in the presence of sodium borohydride ($NaBH_4$) were selected for experiments. The visual photographs and UV-Vis spectroscopic results show that the process of **1a** degraded MB is very complete within 4.5 min. (Fig. 3A), but the degradation of MO, R6G, and RhB dyes is barely changed within this time (Fig. 3B-D). The results suggest that the **1a** exhibit clearly superior catalytic activity for MB dye comparing with MO, R6G, and RhB dyes molecules (Fig. 3E). In addition, when only $NaBH_4$ is added to MB solution, no apparent color change is noted in the methylene blue solution (Fig. S2).

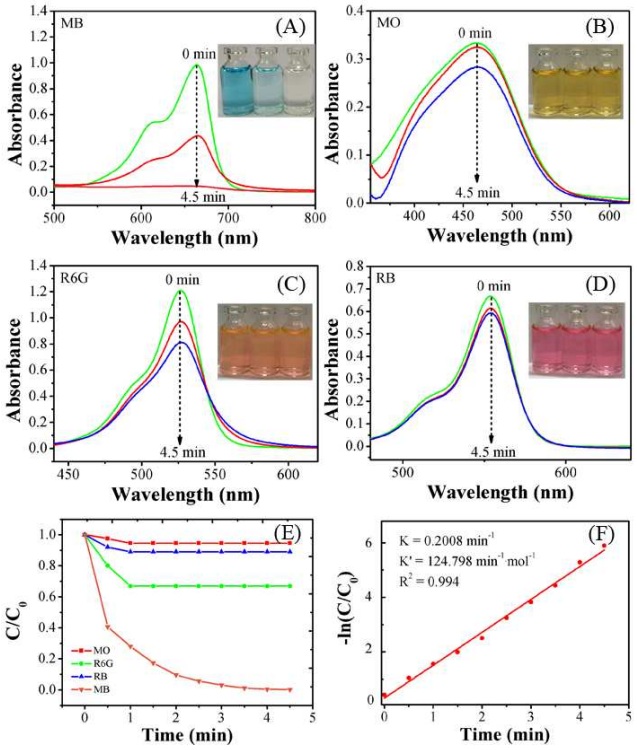

Fig. 3. Successive UV−Vis spectral changes of (A) the 0.01 mM MB solution in the degradation process as a function of the reaction time in the presence of 0.08 mM **1a** and 1.00 mM $NaBH_4$. (B) the 0.01 mM MO solution in the degradation process as a function of the reaction time in the presence of 0.08 mM **1a** and 1.00 mM $NaBH_4$. (C) the 0.01 mM R6G solution in the degradation process as a function of the reaction time in the presence of 0.08 mM **1a** and 1.00 mM $NaBH_4$. (D) the 0.01 mM RB solution in the degradation process as a function of the reaction time in the presence of 0.08 mM **1a** and 1.00 mM $NaBH_4$. (E) The catalytic degradation efficiency of **1a** to MB, MO, R6G, RB. (F) First-order linear relationship between $-\ln(C_t/C_0)$ and reaction time.

Effect of the 1a, $NaBH_4$ concentration and pH.

The influence of **1a** nanocatalyst and $NaBH_4$ concentration on the degradation of MB was also evaluated. When $NaBH_4$ concentration increased from 0.50 to 1.50 mM, the degradation efficiency increased correspondingly from 82 to 99.3%, because of an increase in BH_4^- anions with increasing concentration of $NaBH_4$.[17] However, on increasing $NaBH_4$ concentration from 1.00 to 1.50 mM, the degradation efficiency was almost unchanged (Fig. S3D). From Fig. S3A, it is clear that an increase in the catalytic degradation effciency of MB was observed by increasing the amount of catalyst from 0.04 mM to 0.08 mM in 0.01 mM of the employed solutions of MB. The catalytic degradation efficiency increased slowly as the catalyst dosage increased from 0.04 mM to 0.12 mM. The increased degradation efficiency mainly due to increased catalyst loading, introduced more active sites,[18] consequently, allowing for greater production of the degradation reaction. In our experiments, MB almost completely degraded within 4.5 min at catalyst dosages of 0.08 mM in the presence of $NaBH_4$ (1.00 mM). So, the optimal **1a** nanocatalyst and $NaBH_4$ concentrations were 0.08 and 1.00 mM, respectively (Fig. S3). Thus, subsequent experiments were performed under these conditions. Also, the degradation process is fit for pseudo first-order kinetics by linear fitting according to $\ln(C/C_o) = kt$, where C is the concentration of MB at time t, C_o is the initial concentration of MB (Fig. S3 B, E). The degradation rate and the mineralization percentages are plotted in Fig S3C, with x varying from 0 to 0.12, the degradation activity increases, and it goes continue increasing.[19]

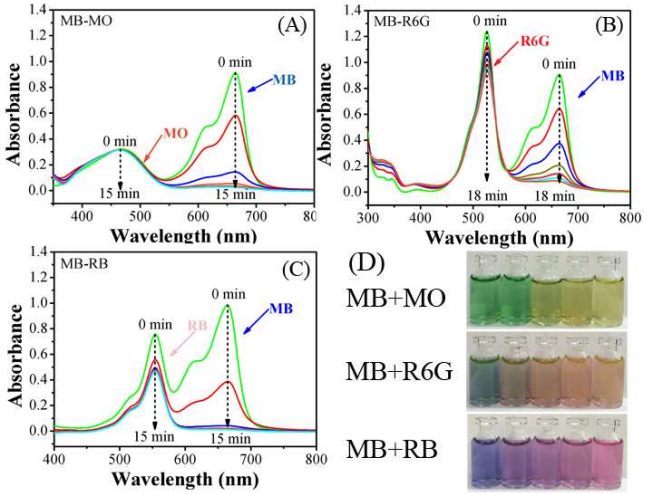

Fig. 4. The selective catalytic activity of **1a** toward the mixed dyes: (A) MB and MO, (B) MB and R6G, (C) MB and RB. (D) The colour changes of the mixed dyes solution before and after degradation using **1a**.

The pH of the solution is one of the significant parameters affecting on the degradation of organic dyes. A series of the solution varying the pH ranges from 2.0 to 13.0 were used the degradation experiments as shown in Fig. S4. The pH solution was prepared with 0.1 M HCl and 0.1 M NaOH. It could notice that pH varying from 4.0 to 8.0, the degradation

efficiency reached an increasing trend. The maximum degradation efficiency occurs at pH 8.0. About 99% of MB was degraded at pH 8.0 after 4.5 min. However, at the lower pH (pH < 4) and the higher pH (pH > 9), MB had little degradation reaction.

3.3 The reaction mechanism and selective study of 1a toward MB

To elucidate the reaction mechanism, the kinetics of the catalytic reaction with respect to MB were studied. The reaction processes were monitored by recording the absorbance intensity changes at 665 nm in a certain period of time at room temperature. In the catalyzed reduction reaction, owing to the fact that the concentration of reductant $NaBH_4$ was much larger than that of MB dye, the reduction reaction could be considered as a pseudo-first-order reaction with regard to MB dye only.[20] The rate constant k was determined by a linear plot of $-\ln(C_t/C_0)$ and reaction time t, where C_t and C_0 are the MB dye concentrations at time t and 0, respectively. C_t/C_0 was measured from the relative intensity of the respective absorbance A_t/A_0. A first-order linear relationship was obtained (Fig. 3F). The rate constant was calculated to be 0.2008 min^{-1} at 25 °C for the reaction catalyzed using **1a** nanocatalyst. For a quantitative comparison, the activity parameter $k' = k/C_M$ was introduced, which is defined as the ratio of the rate constant k to the concentration of the active sites. Among that, $C_M = c \times V$, c was the concentration of **1a** active sites (Cu^{2+} 0.00805 mol/L), V was the optimal volume of **1a** (20 mL) in degradation process. Thus, k' was calculated to be 124.789 $min^{-1}mol^{-1}$ for **1a** nanocatalyst. The bleaching rate is considerably higher than the rates reported previously under similar experimental conditions with noble meatal nanocatalysts.[21] This outstanding catalytic performance could be ascribed to the relatively smaller size of **1a** catalyst.

To further confirm whether **1a** has the ability to selectively degrade MB dyes from mixed dye solution, the mixed dye solution of MB and MO, MB and R6G, MB and RhB were prepared and used (Fig. 4). UV-Vis spectroscopy was measured to determine the degradation capability of **1a** catalyst, which shows that all absorption peaks of MB molecules disappeared quickly, just leaving the characteristic absorption peaks of MO, R6G, and RhB while exposed to the corresponding dye-mixture (Fig. 4A-C). The visual photographs of dye-selective adsorption clearly show that the color change from green color for mixed MB-MO, purple color for MB-RhB, and amaranth color for MB-R6G to pure orange MO, pink RhB, and scarlet R6G solution can be readily observed by the naked eye (Fig. 4D). The result suggests that the **1a** catalyst has high degradation selectivity towards MB against other dyes, obviously attributed to the specific interaction of active sites of catalyst with the MB molecule, allowing the selective degradation of MB from the mixture solution.[22]

3.4 Reusability of the 1a catalyst

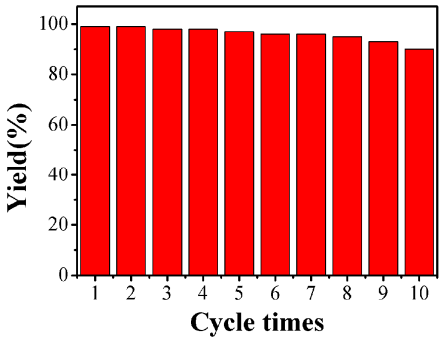

Fig. 5. The reusability of **1a** for the degradation of MB.

In addition to catalytic activity, stability and reusability are another important properties for catalysts as these two properties determine service life of nanocatalyst. To examine the reusability, the **1a** nanocatalyst was isolated from the reaction mixture by an external magnet and reused in the next cycle due to its magnetic property (inset of Fig. 2). As shown in Fig. 5, the **1a** catalyst can be successfully reused in ten repeated processes with a conversion of > 90%, indicating excellent recyclability of the catalyst. The stability of the catalyst was also investigated by measuring the Cu loss after ten successive cycles with ICP-MS. The test showed that there was about 6.73 wt% of Cu in reaction solution after ten cycles, indicating slight leaching of the Cu. Additionally, the XRD spectrum of **1a** nanocatalyst after ten cycles matches well with the as-synthesized product (Fig. S5).

4. Conclusion

In summary, monodisperse $CuFe_2O_4$ NPs have been successfully synthesized, and were adopted for the egradation of dyes in the aqueous solution as catalyst. Interestingly, they not only exhibit high catalytic activity for rapid degradation MB dye, but also realize the fast selective degradation of MB dye from the mixed dye-wastewater (MB and MO, MB and R6G, MB and RB) as is expected. More importantly, the $CuFe_2O_4$ nanocatalyst has a very low leaching loss and excellent reusability for ten catalysis cycles in the degradation of MB, indicating that $CuFe_2O_4$ nanocatalyst could overcome the drawbacks of homogeneous catalysts. Since the current method is simple and flexible to create recyclable catalyst with high stability and excellent selectivity toward dye degradation, this nanocatalyst is an important tool in catalysis, and the selective degradation and recycling of raw material in wastewater.

Notes and references

[a]*College of Chemistry and Chemical Engineering, Northwest Normal University, Lanzhou, Gansu, 730070 (P.R. China). E-mail: songym@nwnu.edu.cn,*

[b]*Key Laboratory of Nonferrous Metal Chemistry and Resources Utilization of Gansu Province, State Key Laboratory of Applied Organic Chemistry, and Key Laboratory of Special Function Materials and Structure Design, Ministry of Education, Lanzhou University Gansu, Lanzhou, 730000 (P.R. China). E-mail: wangbd@lzu.edu.cn.*

[c]*Key Laboratory for New Molecule Material Design and Function of Tianshui Normal University, Tianshui, Gansu 741001, PR China. E-mail: huiantang@163.com*

†Electronic Supplementary Information (ESI) available: [Experimental details, synthesis, characterization, and FT-IR and UV spectra data]. See

DOI: 10.1039/b000000x/
‡The work was supported by the National Natural Science Foundation of China (21271093, 21431002 and 21401091), the National Basic Research Program of China (973 Program) No. 2012CB933102, the Program for New Century Excellent Talents in University (NCET-13-0262), the Fundamental Research Funds for the Central Universities (lzujbky-2014-k06), and education research project of Gansu Province (2013A-102).

1 (a) P. Bautista, A. F. Mohedano, J. A. Casas, J. A. Zazo and J. J. Rodriguez, *J. Chem. Technol. Biotechnol.*, 2008, **83**, 1323-1338; (b) A. H. Xu, X. X. Li, S. Ye, G. H. Yin and Q. F. Zeng, *Appl. Catal., B*, 2011, **102**, 37-43; (c) S. Caudo, G. Centi, C. Genovese and S. Perathoner, *Top. Catal.* 2006, **40**, 207-219.
2 (a) I. Ali, *Chem. Rev*. 2012, **112**, 5073−5091; (b) X. J. Li, Z. Y. Hou, Y. Zhang, G. Zhang, J. S. Lian and J. Lin, *Dalton Trans.*, 2014, **43**, 15457-15464; (c) M. Schlesinger, S. Schulze, M. Hietschold and M. Mehring, *Dalton Trans.*, 2013, **42**, 10471056.
3 (a) M Panizza and G. Cerisola, *Chem. Rev*. 2009, **109**, 6541−6569; (b) P. R. Chowdhury and K. G. Bhattacharyya, *Dalton trans.*, DOI : 10.1039/C5DT00257E; (c) R. G. Chaudhuri and S. Paria, *Dalton Trans.*, 2014, **43**, 5526-5534.
4 (a) P. Padhye and P. Poddar, *J. Mater. Chem. A*, 2014, **2**, 19189-19200; (b) Y. E. Miao, H. K. Lee, W. S. Chew, I. Y. Phang, T. X. Liu and X. Y. Ling, *Chem. Commun.,* 2014, **50**, 5923-5926; (c) D. J. Wang, L. Guo, Y. Z. Zhen, L. L. Yue, G. L. Xue and F. Fu, *J. Mater. Chem. A*, DOI: 10.1039/c4ta01444h; (d) T. J. Yao, T. Y. Cui, H. Wang, L. X. Xu, F. Cui and J. Wu, *Nanoscale*, 2014, **6**, 7666-7674.
5 (a) B. B. Cui, H. Lin, J. B. Li, X. Li, J. Yang and J. Tao, *Adv. Funct. Mater.*, 2008, **18**, 1440-1447; (b) Y. G. Li, P. Hasin and Y. Y. Wu, *Adv. Mater.*, 2010, **22**, 1926-1929; (c) Z. Y. Wang, G. W. Hu, J. Liu, W. S. Liu, H. L. Zhang and B. D. Wang, *Chem. Commun.*, 2015, **51**, 5069-5072.
6 (a) A. Walsh, Y. F. Yan, M. M. Al-Jassim, and S. H. Wei, *J. Phys. Chem. C,* 2008, **112**, 12044-12050; (b) X. L. Yin, H. M. Han, M. Kubo, and A. Miyamoto, *Theor. Chem. Acc.*, 2003, **109**, 190-194; (c) X. L. Xu, W. K. Chen and J. Q. Li, *J Mol. Struct.: THEOCHEM,* 2008, **860**, 18-23; (d) G. Fierro, R. Dragone, and G. Ferraris, *Appl. Catal., B: Environ.*, 2008, **78**, 183-191; (e) D. Fino, N. Russo, G. Saracco, and V. Specchia, *Catal*., 2006, **242**, 38-47.
7 (a) W. F. Shangguan, Y. Teraoka, S. Kagawa, *Appl. Catal., B: Environ.*, 1996, **8**, 217-227; (b) W. F. Shangguan, Y. Teraoka, S. Kagawa, *Appl. Catal., B: Environ.,* 1997, **12**, 237-247; (c) W. F. Shangguan, Y. Teraoka, S. Kagawa, *Appl. Catal., B: Environ.*, 1998, **16**, 149-154; (d) Z. Jiang, W. H. Zhang, W. F. Shangguan, X. J. Wu, and Y. Teraoka, *J. Phys. Chem. C*, 2011, **115**, 13035-13040.
8 (a) W. B. Shi, X. D. Zhang, S. H. He and Y. M. Huang, *Chem. Commun.*, 2011, **47**, 10785-10787; (b) J. Deng, Y. S. Shao, N. Y. Gao, C. Q. Tan, S. Q. Zhou and X. H. Hu, *J. Hazard Mater.*, 2013, **262**, 836-844.
9 (a) J. Liu, W. Zhang, H. L. Zhang, Z. Y. Yang, T. R. Li, B. D. Wang, X. Huo, R. Wang, and H. T. Chen, *Chem. Commun.*, 2013, **49**, 4938-4940; (b) J. Liu, W. Zuo, W. Zhang, J. Liu, Z. Y. Wang, Z. Y. Yang and B. D. Wang, *Nanoscale*, 2014, **6**, 11473.(c) B. D. Wang, J. Hai, Q. Wang, T. R. Li and Z. Y. Yang, *Angew. Chem., Int. Ed*., 2011, **123**, 3119.
10 (a) J. N. Zheng, Z. A. Lin, W. Liu, L. Wang, S. Zhao, H. H. Yang, and L. Zhang, *J. Mater. Chem. B*, 2014, **2**, 6207-6214; (b) M. Y. Zhu, D. H. Meng, C. J. Wang, and G. W. Diao, *ACS Appl. Mater. Interfaces*, 2013, **5**, 6030-6037.
11 (a) C. Singh, A. Goyal and S. Singhal, *Nanoscale*, 2014, **6**, 7959-7970; (b) J. N. Zheng, Z, Lin, W. Liu, L. Wang, S. Zhao and H. H. Yang, *J. Mater. Chem. B*, 2014, **2**, 6207-6214.
12 J. D. Perkins, J. M. Graybeal, M. A. Kastner, R. J. Birgeneau, J. P. Falck, M. Greven, *Phys. Rev. Lett.* **1993**, 71, 1621-1624.
13 F.A. Cotton, G. Wilkinson, *Advanced Inorganic Chemistry*, Interscience Publishers, London, 1974.
14 T. Zhang, H. B. Zhu, and J. –P. Croué, *Environ. Sci. Technol.*, 2013, **47**, 2784-2791.
15 J. X. Zhao, Y. L. Cheng, X. B. Yan, D. F. Sun, F. L. Zhu and Q. J. Xue, *CrystEngComm.*, 2012, **14**, 5879-5885.
16 Y. T. Zhao, G. Y. He, W. Dai, and H. Q. Chen, *Ind. Eng. Chem. Res.*, 2014, **53**, 12566-12574.
17 M. Nemanashi and R. Meijboom, *J. Colloid Interface Sci.*, 2013, **389**, 260-267.
18 (a) S. Mayavan, H. S. Jang, M. J. Lee, S. H. Choi and S. M. Choi, *J. Mater. Chem. A*, 2013, **1**, 3489-3494; (b) D. P. He, K. Cheng, T. Peng, X. L. Sun, M. Pan and S. C. Mu, *J. Mater. Chem.*, 2012, **22**, 21298-21304; (c) B. H. Wu, N. F. Zheng and G. Fu, *Chem. Commun.*, 2011, **47**, 1039-1041.
19 J. Ren, S. X. Ouyang, H. R. Chen, N. Umezawa, D. Lu, D. F. Wang, H. Xu, J. H. Ye, *Applied Catalysis B : Environmental*, 2015, **168-169**, 243-249.
20 E. Lam, S. Hrapovic, E.Majid, J. H. Chong and J. H. T. Luong, Nanoscale, 2012, 4, 997–1002
21 H. W. Hu, J. H. Xin and H. Hu, *J. Mater. Chem. A*, 2014, **2**, 11319-11333.
22 N. Li, X. Hua, K. Wang, Y. J. Jin, J. J. Xu, M. D. Chen and F. Teng, *Dalton Trans.*, 2014, **43**, 13742-13750.